JOURNAL OF GEOPHYSICAL RESEARCH, VOL. 113, F03027, doi:10.1029/2007JF000820, 2008

A methodology for calculating the spatial distribution of the area-slope equation and the hypsometric integral within a catchment

Sagy Cohen,[1,2] Garry Willgoose,[1] and Greg Hancock[2]

Received 23 April 2007; revised 5 May 2008; accepted 13 June 2008; published 23 September 2008.

[1] The area-slope relationship and the hypsometric curve are well known catchment descriptors. The main shortcoming of traditional area-slope and hypsometry extraction methods is their limited ability to represent heterogeneity within the catchment. Here we present a new methodology for explicit calculation of the spatial distribution, at a pixel scale within a catchment, of the area-slope parameters and the hypsometric integral. This method allows us to create a quantitative representation of the area-slope equation and the hypsometric integral which can potentially be used in a variety of geomorphologic applications. The results show that the spatial distribution of both the area-slope equation and the hypsometric integral are noisy at the pixel scale. In order to reduce the noise three averaging techniques were examined. Subcatchment-scale averaging was found to be the best at identifying the spatial distribution of the area-slope equation and hypsometric integral. At the subcatchment scale the spatial distribution of the area-slope equation and the hypsometric integral approximated the spatial distribution of soil morphological and geological units of the Goulburn River catchment in eastern Australia. The spatially distributed area-slope results were tested using manually extracted subcatchment average area-slope values and found to be well correlated. The spatially distributed hypsometric integral was also well correlated with landform concavity and convergence. The subcatchment-scale averaging of the spatially distributed area-slope equation and hypsometric integral is shown to be a promising tool for producing spatially distributed data. The techniques are demonstrated on a catchment that has marked spatial variation in soils and geology. The results show that the spatially explicit maps can potentially identify the spatial extent of these soil types and geological features and agrees well with existing soil maps.

Citation: Cohen, S., G. Willgoose, and G. Hancock (2008), A methodology for calculating the spatial distribution of the area-slope equation and the hypsometric integral within a catchment, *J. Geophys. Res.*, *113*, F03027, doi:10.1029/2007JF000820.

1. Introduction

[2] Soil functional properties vary systematically at the hillslope scale, and distributed process models (e.g., hydrology and erosion) would benefit from maps of soil functional properties for large catchments. For example, *Bloschl et al.* [1995] and *Grayson et al.* [1995] show that the spatial organization of saturated areas at the hillslope scale systematically impacts on the catchment-scale hydrograph. Accordingly there is significant interest in automated methods that can predict the spatial distribution of soil properties at the hillslope scale from easily measured geomorphic properties [*McBratney et al.*, 2003]. Significant progress has been made in the past decade in describing the spatial distribution of area-slope and hypsometry for channels and linking this distribution to dominant channel process [e.g., *Tucker and Whipple*, 2002]. Less progress has been made for describing hillslopes and linking these descriptions to the soil of the hillslopes [e.g., *Minasny and McBratney*, 2001, 2006]. Mapping the spatial distribution of area-slope and hypsometry within a catchment will allow us to explore explicit spatial links between geomorphology and erosion processes, morphology, surface concavity, soil characteristics, geology, etc. This would have direct applicability to digital soil mapping and soil pedogenesis modeling [*Minasny and McBratney*, 2006]. Maps of intracatchment soil spatial distribution would also improve models for hydrology and geomorphology that use the area-slope relationship [e.g., *Willgoose and Perera*, 2001].

[3] In this paper we describe and explore new automated algorithms for calculating the area-slope equation and hypsometric integral at a pixel scale thus providing high-resolution maps of the intracatchment variability of these properties. We also provide a preliminary demonstration of these techniques by predicting the spatial distribution of soils in a test catchment where soils maps are available for comparison.

[1]School of Engineering, University of Newcastle, Callaghan, New South Wales, Australia.
[2]School of Environmental and Life Sciences, University of Newcastle, Callaghan, New South Wales, Australia.

0148-0227/08/2007JF000820$09.00

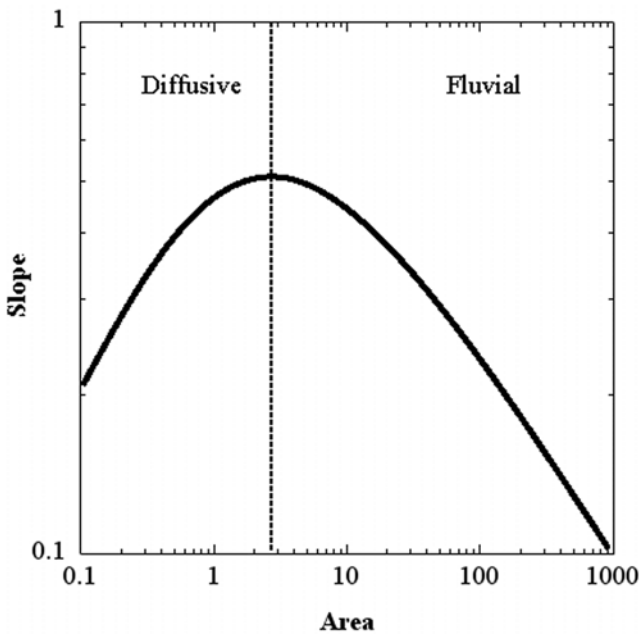

Figure 1. A typical transport-limited area-slope relationship log-log curve. The dashed line indicates the transition point between the diffusive-dominated regions on the left and fluvial-dominated regions on the right.

[4] Researchers have observed and measured the relationship between contributing area and local slope in channels [e.g., *Horton*, 1945; *Hack*, 1957; *Flint*, 1974; *Sklar and Dietrich*, 1998] and hillslopes [*Gilbert*, 1909]. *Flint* [1974] described a general power law relationship between the slope and stream magnitude that is approximately equivalent to

$$S = cA^{\alpha}, \tag{1}$$

where S is the local slope, A is the contributing area, c is a slope-scaling constant and α is the exponent coefficient. In a catchment dominated by transport-limited erosion processes a typical log-log area-slope curve exhibits two distinct regions (Figure 1), a diffusive dominated region on the left-hand side (low area values) and a fluvial dominated region on the right-hand side (high area values [*Willgoose et al.*, 1991; *Willgoose*, 1994; *Hancock and Willgoose*, 2002; *Hancock*, 2005; *Grimaldi et al.*, 2005; *Hancock and Evans*, 2006]). The diffusive region has been interpreted to be dominated by processes such as rainsplash, soil creep and interrill erosion accruing on hillslopes while the fluvial region is associated with channel erosion processes [*Tarboton et al.*, 1992; *Hancock*, 2005; *Hancock and Evans*, 2006]. The two regions are also associated with landform concavity with the diffusive dominated region generating concave down landforms and concave up landforms generated in the fluvial dominated region. *Willgoose et al.* [1991] and *Willgoose* [2001] provided mathematical expressions for the two regions in the catchment. Their numerical solution was based on either (1) assuming dynamic equilibrium in which the tectonic uplift (U) is balanced by the temporal average erosion rate ($\underline{\nabla}\ Q_s$) or (2) assuming spatially uniform erosion equal to U leading to

$$\frac{\partial z}{\partial t} = U + \underline{\nabla Q_s} = 0, \tag{2}$$

where z is the elevation, t is time and Q_s is the sediment flux. An integral solution at any point of the catchment with a known area draining through it (A) leads to

$$UA = Q_s = f_{Q_s}(Q, S) = f_{Q_s}\big(f_Q(A), S\big), \tag{3}$$

where Q is the runoff discharge through a point. This allows us to solve the area-slope relationship for different erosion processes. Using simple sediment flux and discharge equation ($Q_s = \beta_1\ Q^{m_1} S^{n_1}$ and $Q = \beta_3\ A^{m_3}$ respectively) for transport-limited fluvial process in equation (3) leads to the area-slope relationship [*Willgoose et al.*, 1991]

$$S = \left(\frac{U}{\beta_1 \beta_3^{m_1}}\right)^{\frac{1}{n_1}} A^{\frac{1-m_1 m_3}{n_1}} \propto A^{\alpha}, \tag{4}$$

where β_1, m_1, n_1, β_3 and m_3 are parameters that are generally considered, for the purposes of area-slope analyses, constant in space and time and where α is referred to as the area exponent.

[5] On the basis of $Q_s = DS$ [*Gilbert*, 1909] the area-slope relationship for the diffusive erosion process is [*Willgoose et al.*, 1991]

$$S = \left(\frac{U}{D}\right) A_s^{\alpha}, \tag{5}$$

where D is hillslope diffusivity or creep, $\alpha = 1$, and A_s is the specific area (area draining to that point per unit width). The difference between fluvial and diffusive erosion processes that arise from equations 4 and 5 are the constant and exponent of equation 1 (c and α respectively). A similar argument can be followed for detachment limited erosion processes, with the c being a function of uplift and detachment rate, and the α a function of the discharge and slope dependence on detachment [*Moglen and Bras*, 1995]. We can therefore assert that the spatial distribution of c and α within a heterogeneous catchment is significant and a function of erosion process.

[6] The other geomorphic descriptor we will examine in this paper is the hypsometric curve (Figure 2 [*Strahler*, 1964; *Willgoose and Hancock*, 1998]). The hypsometric curve is a nondimensional area-elevation relationship which allows ready comparison of catchments and is traditionally associated with different stages of catchment maturity [*Strahler*, 1964]. *Willgoose and Hancock* [1998] demonstrated a link between the hypsometric curve and different erosion processes, catchment geometry and network form. The hypsometric integral is the area under the hypsometric curve and provides a quantitative value for comparing catchments. *Walcott and Summerfield* [2007] found a strong spatial trend in the distribution of the hypsometric integral and a correlation to the erosion resistance of lithologies. Using *Willgoose and Hancock*'s [1998] classification, a higher hypsometric integral values (greater then 0.5) represent catchments dominated by diffusive erosion processes

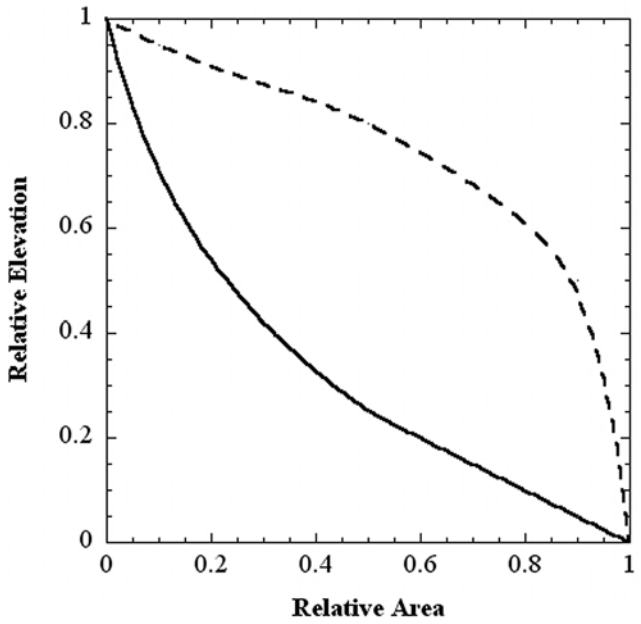

Figure 2. Two typical hypsometric curves. The dashed curve represents a concave down landform associated with diffusive dominated catchments, while the solid line represents a concave up landform associated with fluvial dominated catchments.

(concave down hypsometric curve; Figure 2) while lower values (less then 0.5) represent fluvial dominated catchments (concave up hypsometric curve). We therefore assert that the hypsometric integral is linked to erosion process, and landform curvature and its landscape morphology.

[7] Conventional calculation of the area-slope equation and hypsometric integral requires plotting the relevant variables for a complete catchment and manually extracting either the power law equation of the area-slope curve or the integral of the hypsometric curve. In recent years a more spatially distributed approach has been adopted in channel research. For example, *Seidl and Dietrich* [1992] and *Sklar and Dietrich* [1998] have solved the area-slope equation for principle and tributary channels, *Wobus et al.* [2006] have solved it at channel junctions, while *Brocklehurst and Whipple* [2004] calculated the hypsometric integral in many catchments exploring its variation for different environments. *Walcott and Summerfield* [2007] introduced a new method for calculation of subcatchment hypsometric integral. These recent works while an advance in whole catchment analysis remain spatially limited since most are manually calculated for each catchment (or subcatchment) limiting the number of units investigated and thus the spatial resolution that is practical. By comparison, the spatial distribution of hillslope geomorphic properties and any relationship to soils and/or geology have only been lightly researched [e.g., *Dietrich et al.*, 1993; *Willgoose*, 2001]. Recent advances in GIS based surface analysis tools allow us to develop automated algorithms to solve the area-slope equation and hypsometric integral at a pixel scale within a catchment.

[8] This paper presents a new approach for automatically calculating the spatial distribution of the area-slope parameters and the hypsometric integral at a pixel scale within a catchment thus describing the intracatchment variability. The approach is applied to a large catchment with heterogeneous soils. The resulting, automatically calculated, area-slope parameters are tested against manually extracted area-slope parameters for selected subcatchments on different soils. The hypsometric integral is compared to two independent descriptors of landscape curvature. We will show that the results reveal correlations between the geomorphic parameters and the spatial distribution of soils, morphology and geological features.

2. Study Site

[9] The Goulburn River catchment (approx. 7000 km^2) is located on the Upper Hunter Valley in New South Wales, Australia (Figure 3). The catchment can be divided into the following two distinct geological units:

[10] 1. The northern Basaltic lava region which is a part of the Liverpool Range volcanic province. This region consist of mostly fertile soils [*Galloway*, 1963a] and rolling hills topography (except for the rocky slopes of the Liverpool Range to the extreme north of the catchment) [*Galloway*, 1963b].

[11] 2. The southern Sandstone region dominated by Triassic Sandstones exposed after erosion of the once overlaying basalt layer with a few basalt patches still visible on the cliff tops. Because of its high resistance to erosion the Sandstone region comprises rugged canyon terrain with shallow infertile soils [*Galloway*, 1963a] and wide floodplains along the main channels.

[12] The climate is temperate with average yearly precipitation ranging from 1000 mm in the north to less than 500 mm at the center of the catchment [*Australian Bureau of Meteorology*, 1975]. Temperatures vary between an average minimum of 3°C in the coldest month (July) to an average maximum of 30°C in the hottest (January) [*Australian Bureau of Meteorology*, 1975].

[13] A 25 m square gridded digital elevation model (DEM) of the catchment derived from digitised 10 m contours (from Land and Property Information New South Wales (LPI)) was used for calculating the topographic descriptors in this work. C. Martinez et al. (An assessment of digital elevation models and their ability to capture geomorphic and hydrologic properties at the catchment scale, submitted to *International Journal of Remote Sensing*, 2008) examined the influence of DEM resolution on both area-slope plots and hypsometry of a subcatchment of the Goulburn River catchment located in the center of the study area. Using a range of high-resolution and accurate DEMs (ranging from 5 m resolution created by differential Global Positioning System to the LPI 25 m DEM used in this paper) they found little difference in manually extracted area-slope α and almost no difference in hypsometry. For the entire catchment domain of nearly 11 million cells there were less then 30 000 requiring pit filling, 0.27% of the cells. We are therefore confident in using our 25 m DEM to describe the topography of our study site for our work.

[14] The National Australian soil map (1 km resolution; Figure 3) was used to distinguish between the five dominant soil types in the catchment. The northern basaltic region contains three main soil units: clay-loam on the northern ridges, clay on the central hills and loam in the southern parts. The southern sandstone region contains mostly sandy

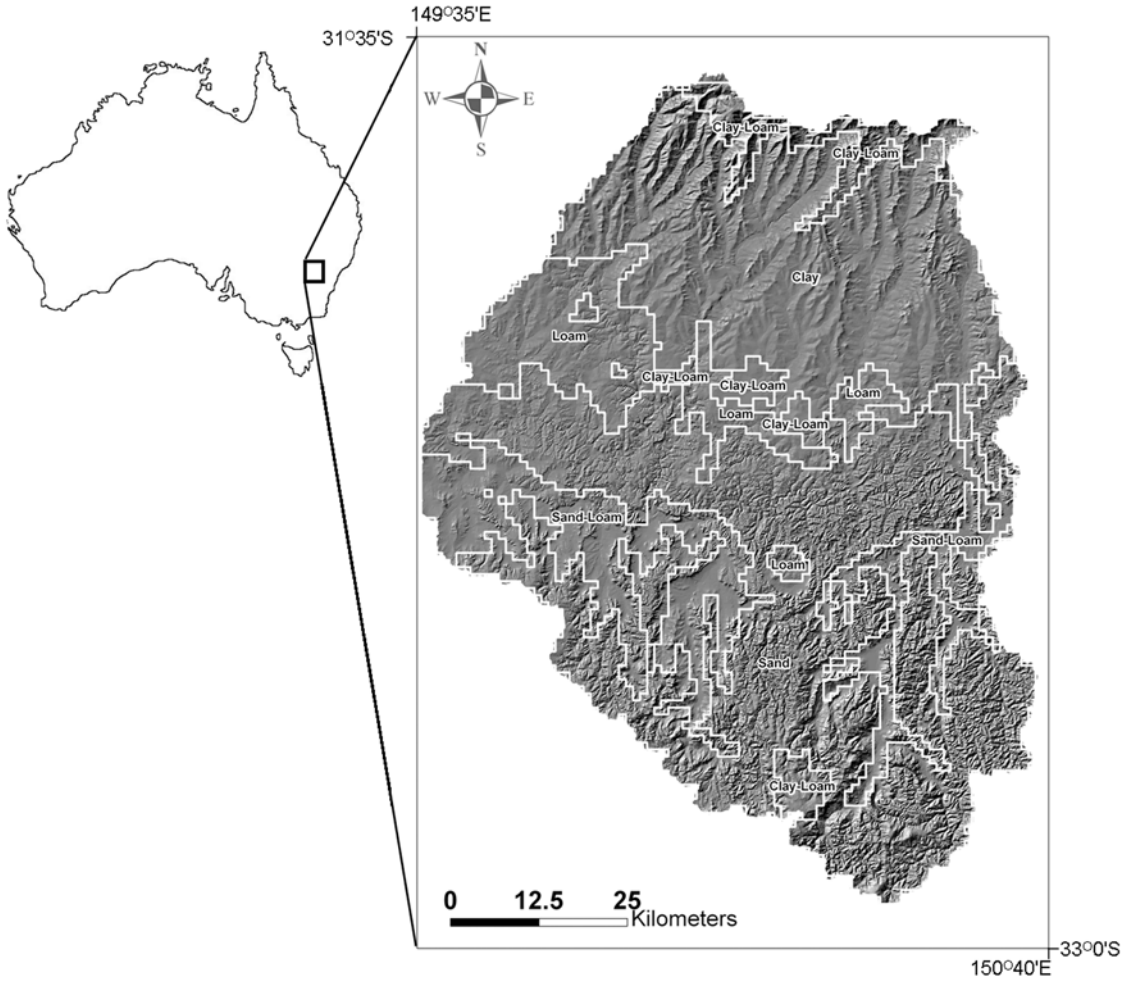

Figure 3. The Goulburn catchment location, relief, and main soil groups. The viewshed presentation of the catchment DEM shows the clear distinction between the rolling hills topography in the northern clay, loam, and clay-loam soils to the rugged terrain in the southern sandy soils and the floodplains dominated by sandy loam soils.

soil with extensive sand-loam strips along the floodplains and a large isolated clay-loam patch in the south. This boundary between the soils of the northern and southern regions is quite sharp, and is easily distinguished in the field and in aerial photos.

3. Spatially Explicit Calculation

3.1. Area-Slope

[15] We based our numeric solution of the area-slope equation on *Seidl and Dietrich*'s [1992] approach. In its simplest form, the spatially explicit solution of equation (1) is based on assuming equal c in two adjacent nodes down the flow path

$$c_i = c_{i+1} = \frac{S_i}{A_i^{\alpha_i}} = \frac{S_{i+1}}{A_{i+1}^{\alpha_i}}, \tag{6}$$

where S_i is the local topographic slope, A_i is the local contributing area, i is the node been calculated and $i + 1$ is the node immediately downstream. The contributing area is the area draining into a node. Rearranging equation (6) leads to

$$\log S_i - \alpha_i \log A_i = \log S_{i+1} - \alpha_i \log A_{i+1}, \tag{7}$$

which is then used to extract α_i

$$\alpha_i = \frac{\log\left(\frac{S_i}{S_{i+1}}\right)}{\log\left(\frac{A_i}{A_{i+1}}\right)}. \tag{8}$$

Parameter c_i is then calculated from equation (6)

$$c_i = \frac{S_i}{A_i^{\alpha_i}}. \tag{9}$$

[16] In this form the spatially explicit algorithm for solving equation (8) and (9) requires the following three input rasters: (1) contributing area (the number of inflowing pixels), (2) local slope, and (3) flow direction (the direction

to the steepest slope neighboring pixel). The flow direction raster is used to determine A_{i+1} and S_{i+1} in equation (8). In this paper we used the Dinf algorithm [*Tarboton*, 1997] to calculate the contributing area map and then the D8 algorithm [*O'Callaghan and Mark*, 1984] to calculate the flow direction raster (used solely to determine the downstream node) since its relative simplicity allows an easier integration into the spatially explicit algorithm programmed in Fortran.

[17] A more algorithmically complicated approach for spatially solving the area-slope equation uses several nodes along the flow path instead of the simple two node approach above. This requires least square regression to average several up and down flow nodes. Each node is then allocated the average area and slope values of its up and down flow node, potentially reducing DEM noise and errors. This method can be applied using as many up and down flow nodes as desired. The main downside of this approach is that it complicates the numerical solution since it requires the inheritance of values from several up and down flow cells instead of the simple use of a flow direction raster in the two node approach. The above calculations were done using a Fortran code with the D8 flow direction raster determined as described above.

3.2. Hypsometric Integral

[18] As previously mentioned, the hypsometric integral is the area under the hypsometric curve (Figure 2). Calculating the hypsometric integral for a single catchment can be simplified by noting that the area under the curve is equal to the area of a rectangle which lies between 0 to 1 on the x axis (relative area) and 0 to mean relative elevation (y axis). Therefore the only variable is the mean relative elevation of a catchment. Our spatial distributed solution for the hypsometric integral then uses the normalization [*Brocklehurst and Whipple*, 2004]

$$\mathrm{HI} = \frac{\overline{Z} - Z_o}{Z_{\max} - Z_o}, \tag{10}$$

where HI is the hypsometric integral, $Z_{\max}$ is the maximum elevation of the catchment, $\overline{Z}$ is the average elevation and Z_o is the minimum or outlet elevation.

[19] The algorithm for spatially explicit calculation of the hypsometric integral solves equation (10) for each pixel in the catchment using a Fortran code. Each pixel is considered a local catchment outlet and the parameters of equation (10) are the elevation characteristics of this local catchment. This algorithm requires the following three input rasters: (1) DEM for extracting the local outlet elevation (Z_o), (2) average elevation ($\overline{Z}$), and (3) maximum elevation ($Z_{\max}$) of the catchment flowing into each pixel. These later two parameters were extracted by a Fortran code.

4. Results

4.1. Area-Slope Parameters

[20] The distinct soil units in Goulburn catchment allow us to more clearly study the correlation between geological and geomorphologic characteristics, and the spatial distribution of α and c. If our hypothesis that geomorphic parameters are related to soil type is correct then the distinct boundaries between the soil types implies that our spatially distributed analyses should also yield distinct regions. The area-slope plot in Figure 4 was created by averaging the slope values of all the pixels with similar area value. For example, the point for area = 1 (i.e., one pixel) is the average slope of all the pixels in the catchment with this area value. This technique enables us to avoid plotting the whole pixel-scale database (over 10×10^6 pixels). It also reduces noise and scatter in the plots so that we can better observe mean trends. This technique is used for all the spatial distributed plots in this paper. Figure 4 shows distinct differences in the area-slope parameters between the different soil units. The clay, clay-loam and loam curves (typically found on the northern part of the catchment) have generally higher α values compared to the sand and sand-loam curves and their y intercept values (c) are generally higher. Figure 4 demonstrates that distinguishing between the different soil units and even between the two major geological groups is not possible in all parts of the plot using either α or c separately, nor that for that matter slope on its own. This suggests that both α and c are needed and that together they provide more spatial information than contributing area or slope values alone.

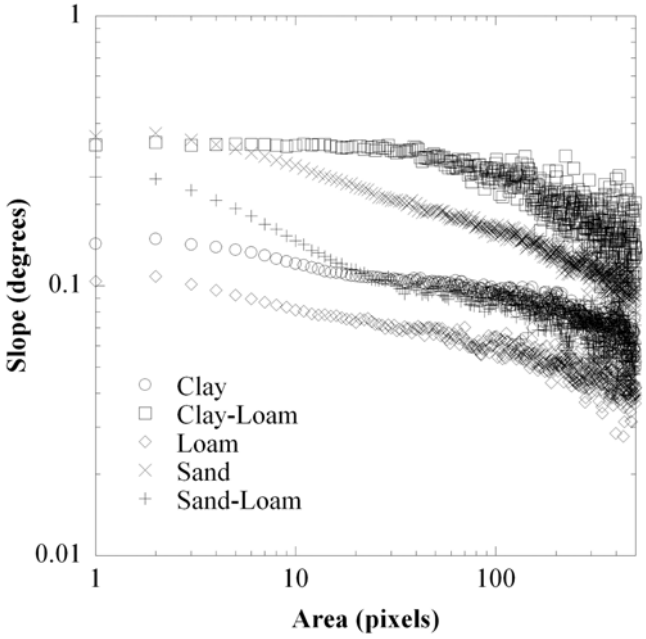

Figure 4. The area-slope relationship for each soil unit in the Goulburn River catchment. Each point is the average slope for all pixels with the same area.

4.1.1. Spatial Distributed α

[21] The spatially distributed α raster exhibits considerable noise with unreasonably high and low extreme values. Those extreme values are the result of small differences in slope, or jumps in the contributing area between two adjacent pixels. Although it may be a natural feature, and despite the fact that they account for a small proportion of pixels (approx. 2%), they severely mask the majority of reasonable values because of their high value (up to a factor of 3). In order to deal with those extreme values we constrained the α values between assigned minimum and maximum thresholds. We examined the following two

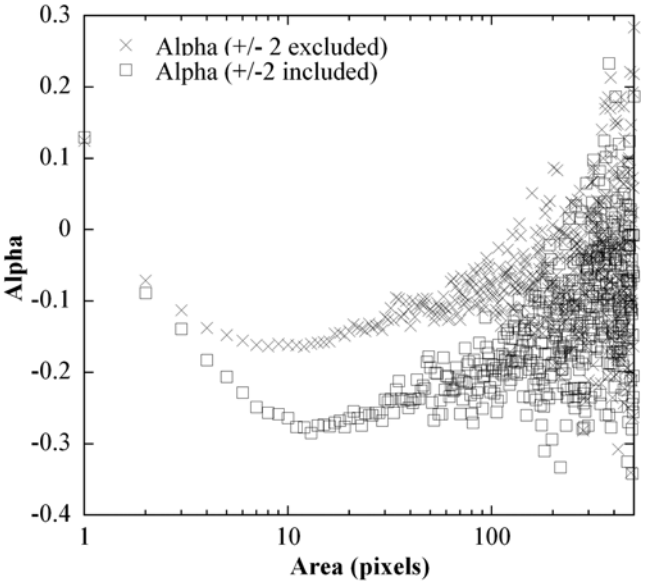

Figure 5. Area-slope relationship of the two constrained α methods. Each point is the average slope for all pixels with the same area. Method 1 (crosses) excluded all outliers larger than 2 and smaller than -2. Method 2 (squares) limited the outliers to fit between 2 and -2 (higher or lower values were assigned with the maximum and minimum value, respectively).

constraint approaches: (1) excluding the extreme values by assigning a "no data" value and (2) including them by assigning a maximum or minimum threshold value. The sensitivity of the threshold value was explored by executing the spatially explicit α algorithm with a range of thresholds, finding the one that resulted in the best fit to the α values that we extracted from the area-slope plot (Figure 4). The threshold values we found to be the best fits were ±2.

[22] We used the threshold value in the two constraining methods and compared the three resulting area-α plots (unconstrained and two constrained methods). Significant differences were found. The unconstrained area-α plot shows considerable scatter and no distinct differences between the five soil types while the two constrained α rasters exhibited a much cleaner plot. The area-α curve of constraint method 2 shows lower values than method 1 (Figure 5) and better represents the manually extracted α values from the area-slope plot. We therefore used method 2 for the remaining analysis.

[23] The area-α plot for constraint method 2 (Figure 6) clearly distinguishes between the two major geological units but still shows considerable scatter for higher area. The α spatial distribution raster (Figure 7a) shows that while constraining the extreme α values reduces the noise so that the spatial pattern is clearer, a visual identification of morphological, geological or soil units remains difficult.

[24] In order to reduce the noise three smoothing techniques were explored. In the first technique, least square regression was used in the spatially explicit algorithm (section 3.1). We examined the use of least square averaging over 3 (one up and one down flow) and 5 pixels (two up and two down flow). The result did not significantly reduce the noise.

[25] In the second technique a low-pass filter was applied. A low-pass filter removes noise by averaging the values of a fixed sized pixel window. We used a 3×3 pixel window. The resulting raster was smoother and improved our ability to identify spatial patterns but still contained considerable noise.

[26] In the third technique α was averaged at a subcatchment scale. The subcatchment layer was calculated from a 25 m DEM using the TauDEM (D. G. Tarboton, Terrain Analysis Using Digital Elevation Models (TauDEM), Utah State University Logan, 2006, available at: http://hydrology.neng.usu.edu/taudem) tools package embedded into ArcGIS. We used Strahler channel order as a threshold variable controlling the scale of the subcatchments. Selecting a lower channel order results in smaller subcatchments and therefore more subcatchments per catchment. We examined a range of channel orders and found that the fourth order resulted in a layer with too much detail (over 40 000 subcatchments), while the eight order resulted in too few with less then 90. We therefore averaged α in three subcatchment layers fifth, sixth, and seventh channel order (containing 9067, 1883, and 381 subcatchments, respectively; Figures 7b–7d). This selection is subjective and we expect the appropriate scale to vary between different catchments and applications. For example, *Walcott and Summerfield* [2007] found order 2–6 subcatchments to be the most appropriate for their hypsometric integral study.

[27] Our subcatchment averaging merges the channel and hillslope pixels despite the potentially different statistics for each regime. We are confident doing so since channelized pixels account for only 1–3% of the catchment area so that the effect of channel-hillslope mergence is statistically negligible. We tested this approximation by removing

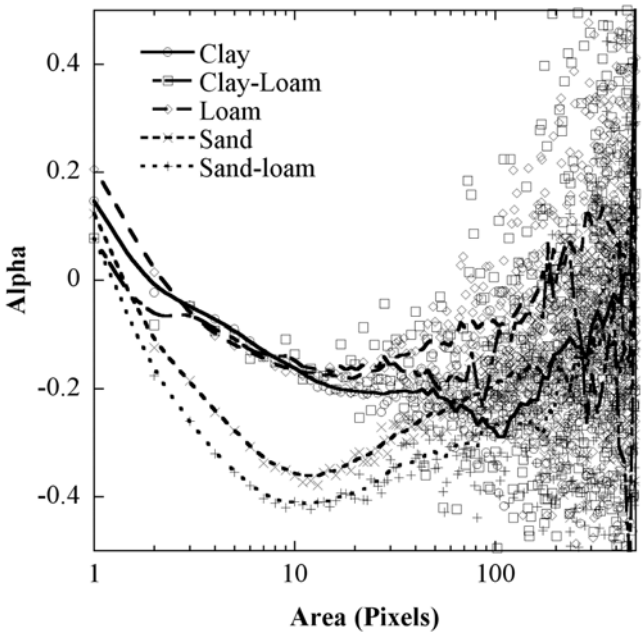

Figure 6. Area-α relationship for each soil unit using constrained α method 2. Each point is the average α for all pixels with the same area. A clear difference can be observed between the northern soil units (clay, clay-loam, and loam) and the southern units (sand and sand-loam) for the lower area values.

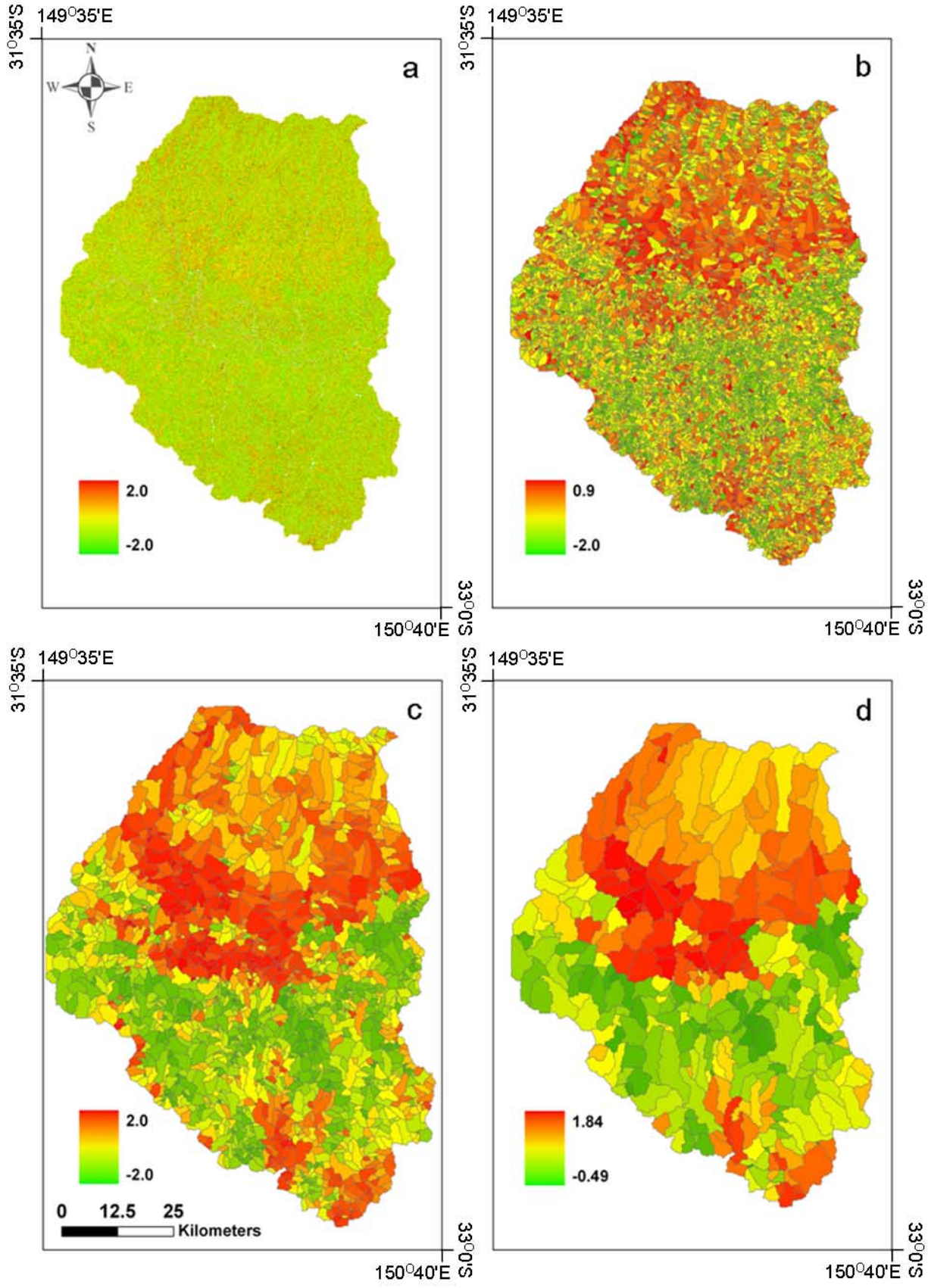

Figure 7. Spatially distributed parameter α for (a) pixel scale and (b) fifth, (c) sixth, and (d) seventh channel order subcatchment scale. For the subcatchment-scale maps (Figures 7b–7d) the value of each subcatchment is the average of the pixels within its boundaries.

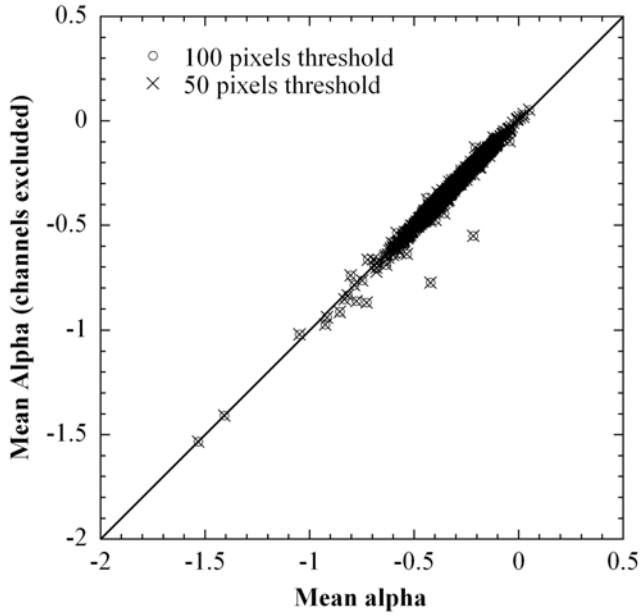

Figure 8. Subcatchment-averaged α using all pixels versus subcatchment-averaged α excluding channelized pixels form two channels maps (calculated by using 100 and 50 pixels thresholds).

channelized pixels from the α map and comparing it to the original map where channels are included. We repeated this exercise for two channel network maps with different contributing area threshold (50 and 100 pixels). These new α maps were averaged in the same way as the original map and compared to the original results. There is a nearly perfect linear correlation ($R^2 > 0.98$; slope = 1.03; interaction <0.01) between the maps at both channel networks (Figure 8). This shows that in our methodology the effect of distinguishing between channel and hillslope is not critical and that the results are insensitive to the channel network or its support area definition.

[28] Figure 7 shows the influence of increasing the scale of averaging on the spatial distribution of α within the Goulburn catchment. At the pixel scale (Figure 7a) a distinction can be made between the northern and southern geological regions but the map is too noisy to allow a clear classification. In the fifth-order subcatchments (Figure 7b) a clear pattern of α distribution emerges with high values in the catchments' northern part and in two distinct clusters in its most southern part. Noise is still apparent at this scale with significant subcatchment to subcatchment variation. This variation may be real but we suspect that it is more likely to be noise. The noise is reduced in the sixth-order subcatchments layer (Figure 7c) and a more distinct classification emerges with higher α value on the clay and loam regions and low values at the sand and sand-loam. At the seventh-order subcatchments layer (Figure 7d) a clear border can be drawn between the morphological units on the basis of the α spatial distribution calculation. At this scale very little noise is apparent but the resolution decreases to only 381 units.

[29] The classification shown by the subcatchments layers corresponds well with the soil map and but less with morphology (Figure 3). This distribution can be interpreted by the fact that Basalt originated soils (clay, clay-loam, and loam) are relatively erosive resulting in smooth topography (rolling hills) which, at a subcatchment scale, has a less convergent flow regime and is therefore more diffusive dominated. As described earlier we expected higher α values in diffusive dominated regions which agree well with our results. Sandstone is highly resistant to erosion which results in a rugged landscape. The soils originated from it (sand and to a lesser extent sand-loam) are therefore expected to be found in fluvial dominated subcatchments. We expect fluvial dominated regions to have lower α values as seen at the subcatchments maps. This classification also corresponds well with the area-slope and area-α plots (Figures 4 and 6, respectively), showing a clear distinction between the sand unit, and the clay and loam units with distinctly lower values in the former. The main deviation from this classification is a high value cluster in the southeast corner of the catchment (Figure 6) which despite its rugged terrain and sandy soils has high α values.

4.1.2. Spatial Distributed *c*

[30] Compared to α, the spatially distributed c raster has less noise at both pixel and subcatchment scale (Figure 9). The area-c plot (Figure 10) shows quite a strong similarity to the area-slope plot (Figure 4) in distinguishing between the soil units. This indicates that the c values alone are unable to distinguish between the soil in all cases. For example the clay-loam curve is relatively similar to the sand curve. The resemblance in shape and values between the area-slope and area-c plots also indicates that a strong correlation exists between slope and c as expected from the form of the area-slope relationship. Correlation analysis between the two

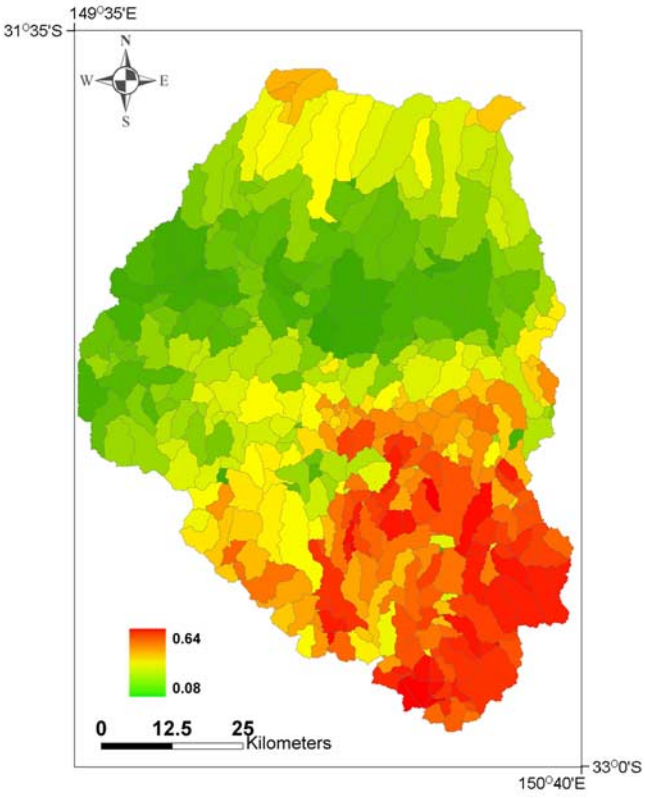

Figure 9. Averaged spatially distributed parameter c for the seventh-order subcatchments. The value of each subcatchment is the average of the pixels within its boundaries.

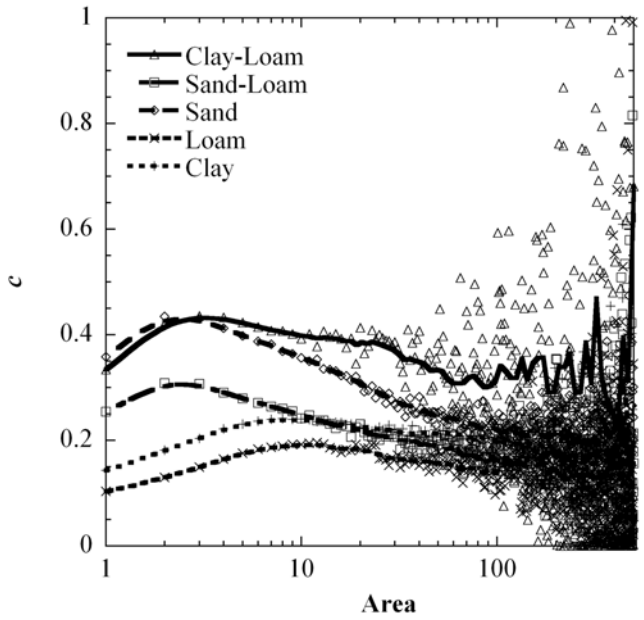

Figure 10. Area-c relationship for each soil unit. Each point is the average c for all pixels with the same area. Show close recumbence to the area-slope plot (Figure 4).

parameters was performed for the following two resolutions: (1) pixel scale and (2) subcatchment scale. For the pixel-scale analysis we used the ArcInfo correlation function which performs a pixel to pixel comparison. In the subcatchment scale the mean c was plotted against mean slope in each subcatchment (at the sixth order). The analysis revealed a relatively high correlation at the pixel scale ($R = 0.52$) which is significantly increased at the subcatchment scale ($R = 0.98$; Figure 11).

[31] The spatial distribution shown in the subcatchment scale (Figure 9) corresponds well with morphology but less well with the soil map. The midnorthern region (dominated by clay and loam soils) as well as the floodplains in the west (dominated by sand-loam soils) received low values as expected in flatter and therefore diffusive dominated regions. On the other hand the steep northern ridges (dominated by clay-loam soils) and the rugged sandstone regions in the southeast received higher values as expected in fluvial dominated regions.

4.1.3. Validation

[32] In order to validate the spatially distributed area-slope parameters, 11 subcatchments (from the seventh-order layer) were randomly selected from across the five soil regions. We then plotted the area-slope relationship for each one and manually extracted α and c by calculating the power law equation of the log-log curve. This is the traditional calculation method that provides a single lumped value for α and c for the catchment. The manually extracted α and c were compared with our averaged spatially distributed α and c in each of the 11 subcatchments. Figure 12 reveals a good correlation for both α ($R = 0.79$) and c ($R = 0.97$) confirming the validity of our pixel-based method.

4.2. Hypsometric Integral

[33] As for the area-slope parameters the hypsometric integral raster exhibits noise at the pixel scale which decreases when averaged to the subcatchment scale (Figure 13). While generally similar, the spatial distribution of the subcatchment layer in Figure 13 shows a different pattern than for α and c (Figures 7 and 9) in some parts of the catchment. The hypsometric integral provides a clearer distinction between the northern and southern regions of the catchment (i.e., basalt and sandstone regions) with the northern region containing higher values which corresponds well with the diffusive dominated regime. However, it does not differentiate between the soils units within each geological region. This inability to differentiate is also shown in the area-hypsometric-integral plot (Figure 14) which fails to clearly distinguish between the soil units.

[34] *Willgoose and Hancock* [1998] indicate that the hypsometric integral is associated with the landform concavity. We used the ArcInfo Curvature tool to create a curvature raster which quantitatively represent the upward or downward curvature of a pixel relative to its eight neighbors. The correlation between the hypsometric integral and the curvature raster was performed at a pixel scale and subcatchment scale using the same method as in α and c correlation analysis as described earlier. The analysis reveals only a moderate correlation at both pixel ($R = -0.425$) and subcatchment scales ($R = -0.479$; Figure 15).

[35] The hypsometric integral was also compared to a junction raster. The junction raster is the number of flow paths flowing into a single pixel (Figure 16). The junction raster was calculated by our Fortran software, counting the number of neighboring pixels which flow into each cell. For example a hilltop pixel which has no upslope neighbors has a value of 0. A diffusion dominated catchment will have fewer junctions than a fluvial dominated since hillslope flow paths tend to flow parallel to one another with less intersections than the convergent flow paths typical of channelized flow. We therefore expect a negative relationship between the hypsometric integral and junctions since the

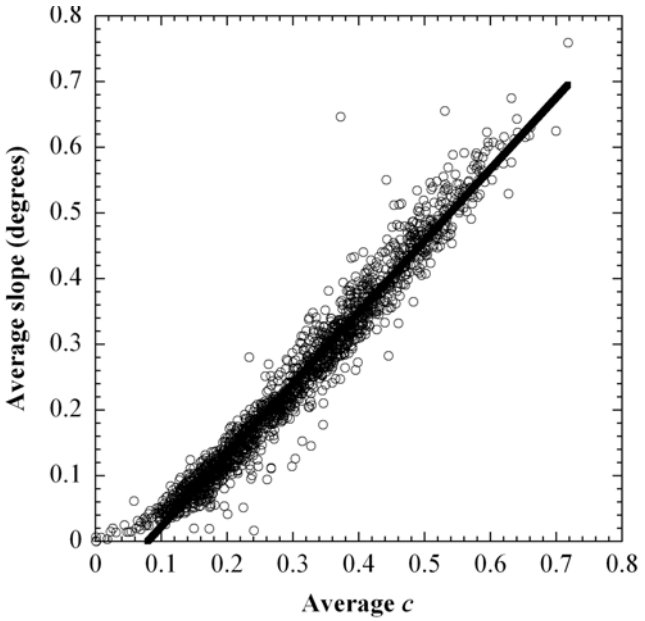

Figure 11. Averaged c versus averaged slope for the sixth-order-scale subcatchments. The linear fit curve equation is $y = -0.085 + 1.088x$ and $R = 0.981$.

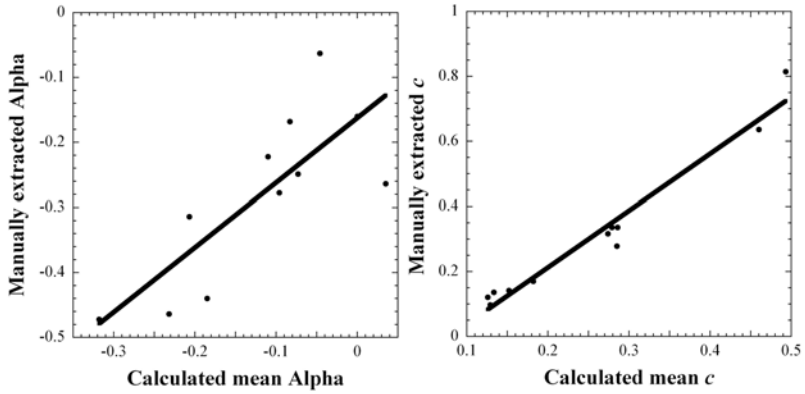

Figure 12. Manually extracted versus averaged spatially distributed (left) α and (right) c for 11 randomly selected subcatchments. The linear fit curve equation is $y = -0.162 + 0.995x$ and $R = 0.792$ for Figure 12 (left) and $y = -0.136 + 1.745x$ and $R = 0.979$ for Figure 12 (right).

hypsometric integral should have larger values for diffusive dominated catchments and lower values in fluvial dominated catchments (as seen in the spatial distribution map; Figure 13). The correlation analysis was done by averaging the hypsometric integral and junctions in each of the sixth-order subcatchments. The resulting plot (Figure 17) shows a good negative correlation ($R = -0.756$).

5. Discussion

[36] Overall, subcatchment averaging showed a good correlation with the soil map and the main geological features, and was the best of three smoothing techniques tested. Differences in the size of subcatchments influenced the amount of noise and the ability to classify the soil and the morphological variety. An increase in subcatchment size improved signal to noise but reduced the spatial resolution. The difference between the two major soil units (sand and clay) which represent the dominant geological features of the catchment was found to be statistically significant (at 5% level using a standard t test; Table 1) at subcatchment scale for the area-slope α and c and the hypsometric integral. Those observations suggest that the spatially distributed subcatchment based method can be used to classify and quantify the spatial distribution of morphology and geology of a complex catchment.

[37] Both α and c were found to be well correlated to manually extracted values at a subcatchment scale. This confirms that our new spatially distributed algorithm reliably predicts these two parameters when averaged over

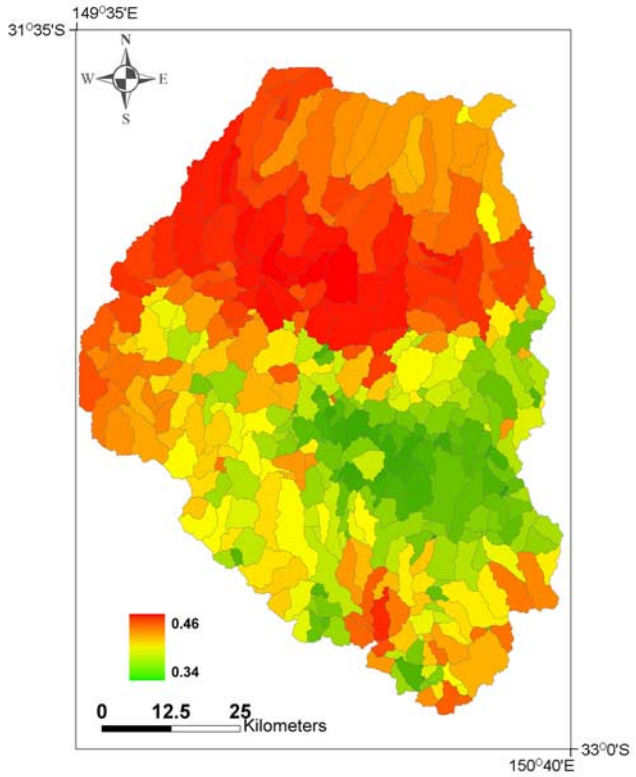

Figure 13. The averaged hypsometric integral for the sixth-order subcatchments. The value of each subcatchment is the average of the pixels within its boundaries.

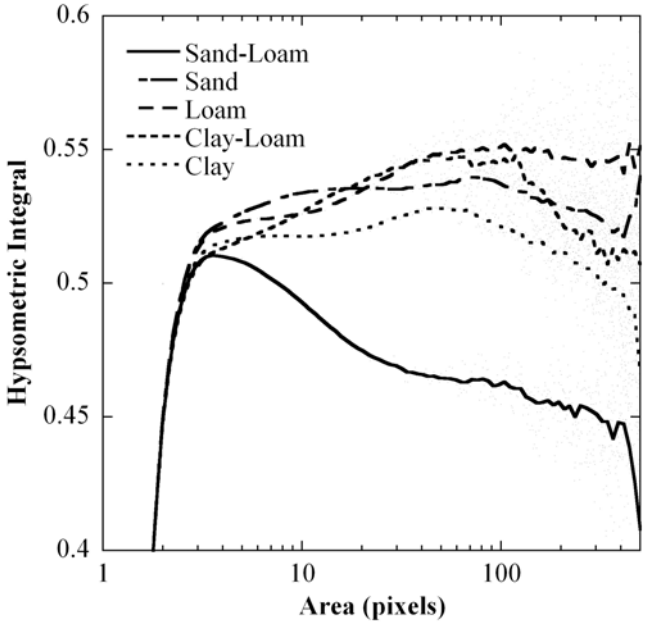

Figure 14. Area-hypsometric-integral relationship for each soil unit. Each point is the average hypsometric integral value for all pixels with the same area.

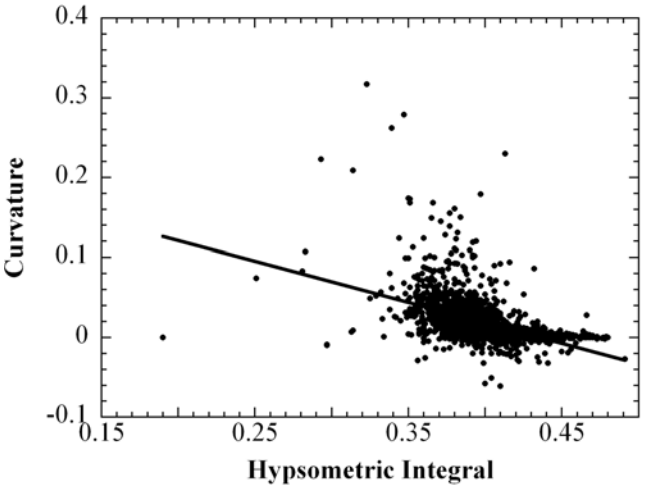

Figure 15. Subcatchment-averaged hypsometric integral versus subcatchment-averaged landform curvature. The linear fit curve equation is $y = 0.224 - 0.515x$ and $R = -0.479$.

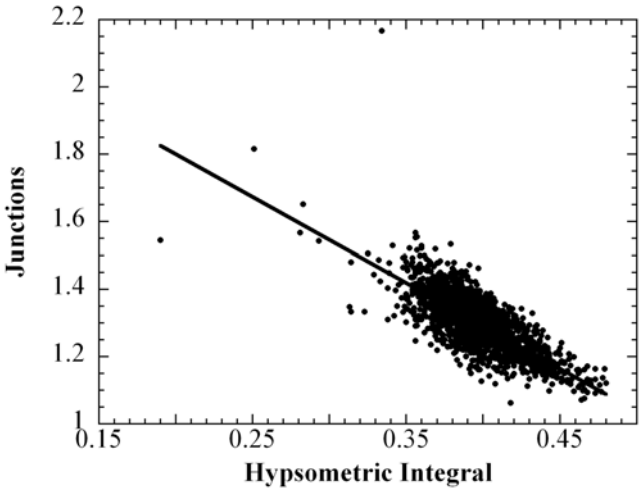

Figure 17. Subcatchment-averaged hypsometric integral versus subcatchment-averaged junctions. The linear fit curve equation is $y = 2.309 - 2.543x$ and $R = -0.756$.

subcatchments. At a subcatchment-scale α agrees well with the soil map while c is better correlated with morphology. As seen on the area-slope plot for each soil unit (Figure 4) α and c individually cannot distinguish between soil morphology for all cases. These observations suggests that a combination of α and c is needed for mapping of soil morphology. An integration of spatially explicit α and c potentially provides added spatial analysis capabilities and needs to be further investigated.

[38] The spatially distributed hypsometric integral calculation showed spatial noise similar to that observed for the area-slope parameters even though its numerics are fundamentally different. Although the hypsometric integral is a less direct measurement of catchment characteristics, taking into account only the elevation variability, it was better able to differentiate between the two main geological units of the catchment and appeared to be more robust in the presence of DEM noise. This is consistent with the spatial correlation found by *Walcott and Summerfield* [2007] between subcatchment hypsometric integral and erosion resistance. This can be explained by the differences between the erosive proporties of the two dominant geological features of the catchment; Basalt which is more erosive resulting in smoother therefore diffusive dominated landscape as appose to the sandstone which is less erosive resulting in rugged therefore fluvial dominated region.

[39] A relatively strong correlation, at the subcatchment scale, was found between the hypsometric integral and a junction raster, an independent measurement of landform morphology related to topographic curvature and is thus related to the dominant erosion process. This strong correlation agrees well with our general hypothesis regarding the link between hypsometric integral and geological features since a more convergent landscape is associated with dominance by fluvial processes resulting in a smaller hypsometric integral while a less convergent landscape is associated with diffusive processes and a larger hypsometric integral. This observation is also consistent with the link between hypsometric integral and the dominant erosion processes proposed by *Willgoose and Hancock* [1998].

[40] The correlation found between hypsometric integral and landform curvature at a pixel scale also corresponds relatively well with *Willgoose and Hancock* [1998] who showed a process link between the hypsometric curve and catchment concavity. It implies that the observation of

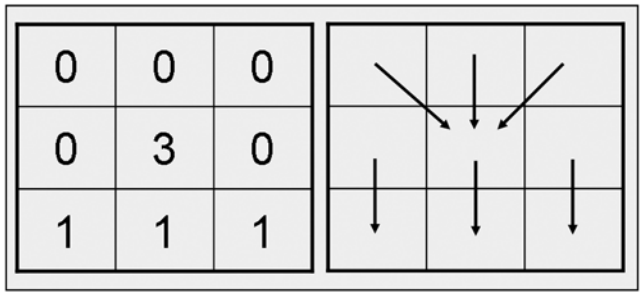

Figure 16. Schematic of the junction raster calculation. The pixel value (the left-hand side raster) is a function of the number of inflowing neighboring cells. The top row and two side pixels in the middle row are 0 since no pixels flow into them. The middle pixel is 3 since all three top row pixels flow into it.

Table 1. Summary of t Test Analysis Parameters Between Clay and Sand Subcatchments (Sixth Order) for Area-Slope Parameters and the Hypsometric Integral[a]

	Mean	Standard Deviation	Number of Points	t Probability
α sand	−0.16	0.14	1307	<.0001
α clay	−0.062	0.085	362	<.0001
c sand	0.362	0.142	1307	<.0001
c clay	0.212	0.091	362	<.0001
HI sand	0.378	0.044	1307	<.0001
HI clay	0.415	0.044	362	<.0001

[a]Here α and c are area-slope parameters and HI is the hypsometric integral.

Willgoose and Hancock [1998] at a catchment scale also applies at an intracatchment scale.

6. Conclusions

[41] A novel approach to area-slope and hypsometry calculation was presented here. It uses an algorithm to calculate the area-slope slope-scaling constant and exponent c and α, and the hypsometric integral in a spatially explicit manner. A pixel-scale solution was found to be too noisy, in this case, for a satisfactory qualitative and quantitative analysis. Averaging the input values along the flow paths and by a simple moving average filtering of the output raster did not significantly improve the noise. Only when the outputs were averaged at a subcatchment scale did distinct spatial distribution patterns emerge. The quality (both the noise and the resolution) of the output map was found to be sensitive to the subcatchments scale.

[42] Our analysis revealed good correlation between the spatially distributed and the manually extracted α lumped at the subcatchment scale and even higher correlation was found for c. Significant differences were found between α and c in terms of their links to spatial features. The area-slope coefficient, α, was better linked to the soil units of the Goulburn River catchment and c was found to be better linked to topography. This suggests, as does the area-slope plots of the soil units (Figure 4), that a combination of the two will allow a significantly improved ability to spatially describe soil and morphology. This idea invites further investigation for a broader range of catchment and soils.

[43] The spatially distributed solution of the hypsometric integral is an indirect measurement of local catchment characteristics. Even with its relative simplicity and indirect link to erosion processes it produced a robust classification of the main geological units of the Goulburn River catchment. While the hypsometric integral has only a moderate correlation with the landform concavity it had a good correlation with another indirect catchment descriptor, a junction raster. Those correlations correspond with the observations of *Willgoose and Hancock* [1998] regarding the influence of different erosion processes on the hypsometric integral.

[44] The finding that there is little difference in the calculated geomorphic parameters for channel networks defined for a range of support areas demonstrates that there is no need to accurately define channel networks for such catchment-scale analysis, and that our methodology is robust against inaccurate channel definition. This greatly simplifies the future application of the approach used here.

[45] At this initial stage there is insufficient data to derive quantitative relations between the area-slope parameters, the hypsometric integral and geomorphological processes rates. However, it is clear from our results that a spatial link between α, c and the hypsometric integral and soil, morphology and geology exist. Despite the noisy nature of α, c and hypsometric integral at a pixel scale, the subcatchment based spatially distributed methods described in this paper show great potential for representing the intracatchment variability of those parameters at a variety of scales. Work still need to be done in order to investigate the brother applicability of this method but the potential is clear.

[46] **Acknowledgments.** We acknowledge the financial support of Australian Research Council grants DP0667093 and DP0556941; S.C. is partially supported by a University of Newcastle Faculty of Science Ph.D. scholarship, and G.W. is supported by an Australian Professorial Fellowship.

References

Australian Bureau of Meteorology (1975), *Climatic atlas of Australia*, Aust. Gov. Print. Serv., Canberra.

Bloschl, G., R. B. Grayson, and M. Sivapalan (1995), On the representative elementary area (REA) concept and its utility for distributed rainfall-runoff modeling, *Hydrol. Process.*, *9*, 313–330, doi:10.1002/hyp.3360090307.

Brocklehurst, S. H., and K. X. Whipple (2004), Hypsometry of glaciated landscapes, *Earth Surf. Processes Landforms*, *29*(7), 907–926, doi:10.1002/esp.1083.

Dietrich, W. E., C. J. Wilson, D. R. Montgomery, and J. McKean (1993), Analysis of erosion thresholds, channel networks, and landscape morphology using a digital terrain model, *J. Geol.*, *101*, 259–278.

Flint, J. (1974), Stream gradient as a function of order, magnitude, and discharge, *Water Resour. Res.*, *10*(5), 969–973, doi:10.1029/WR010i005p00969.

Galloway, R. (1963a), Geology of the hunter valley, in *General Report on the Lands of the Hunter Valley*, *Land Res. Ser.*, vol. 8, edited by R. Story et al., pp. 81–88, Commonw. Sci. and Ind. Res. Organ., Melbourne, Victoria, Australia.

Galloway, R. (1963b), Geomorphology of the hunter valley, in *General Report on the Lands of the Hunter Valley*, *Land Res. Ser.*, vol. 8, edited by R. Story et al., pp. 90–100, Commonw. Sci. and Ind. Res. Organ., Melbourne, Victoria, Australia.

Gilbert, G. (1909), The convexity of hillslopes, *J. Geol.*, *17*, 344–350.

Grayson, R. B., G. Blöschl, and I. D. Moore (1995), Distributed parameter hydrologic modelling using vector elevation data: Thales and TAPES-C, in *Computer Models of Watershed Hydrology*, edited by V. P. Singh, pp. 669–695, Water Resour., Highlands Ranch, Colo.

Grimaldi, S., V. Teles, and R. L. Bras (2005), Preserving first and second moments of the slope area relationship during the interpolation of digital elevation models, *Adv. Water Resour.*, *28*(6), 583–588, doi:10.1016/j.advwatres.2004.11.014.

Hack, J. (1957), Studies of longitudinal stream profiles in Virginia and Maryland, *U. S. Geol. Surv. Prof. Pap.*, *292*, 45–97.

Hancock, G. R. (2005), The use of digital elevation models in the identification and characterization of catchments over different grid scales, *Hydrol. Processes*, *19*(9), 1727–1749, doi:10.1002/hyp.5632.

Hancock, G. R., and K. G. Evans (2006), Channel head location and characteristics using digital elevation models, *Earth Surf. Processes Landforms*, *31*(7), 809–824, doi:10.1002/esp.1285.

Hancock, G. R., and G. R. Willgoose (2002), The use of a landscape simulator in the validation of the Siberia landscape evolution model: Transient landforms, *Earth Surf. Processes Landforms*, *27*(12), 1321–1334, doi:10.1002/esp.414.

Horton, R. (1945), Erosional development of streams and their drainage basin; hydrophysical approach to quantitative morphology, *Geol. Soc. Am. Bull.*, *56*, 275–370, doi:10.1130/0016-7606(1945)56[275:EDOSAT]2.0.CO;2.

McBratney, A. B., M. L. M. Santos, and B. Minasny (2003), On digital soil mapping, *Geoderma*, *117*, 3–52, doi:10.1016/S0016-7061(03)00223-4.

Minasny, B., and A. B. McBratney (2001), A rudimentary mechanistic model for soil formation and landscape development II. A two-dimensional model incorporating chemical weathering, *Geoderma*, *103*, 161–179, doi:10.1016/S0016-7061(01)00075-1.

Minasny, B., and A. B. McBratney (2006), Mechanistic soil-landscape modelling as an approach to developing pedogenetic classifications, *Geoderma*, *133*(1–2), 138–149, doi:10.1016/j.geoderma.2006.03.042.

Moglen, G. E., and R. L. Bras (1995), The effect of spatial heterogeneities on geomorphic expression in a model of basin evolution, *Water Resour. Res.*, *31*(10), 2613–2623, doi:10.1029/95WR02036.

O'Callaghan, J. F., and D. M. Mark (1984), The extraction of drainage networks from digital elevation data, *Comput. Vision Graphics Image Process.*, *28*(3), 323–344, doi:10.1016/S0734-189X(84)80011-0.

Seidl, M. A., and W. E. Dietrich (1992), The problem of channel erosion into bedrock, *Catena Suppl.*, *23*, 101–124.

Sklar, L., and W. Dietrich (1998), River longitudinal profiles and bedrock incision models: Stream power and the influence of sediment supply, *Rivers Over Rock: Fluvial Processes in Bedrock Channels*, *Geophys. Monogr. Ser.*, vol. 107, edited by K. J. Tinkler and E. E. Wohl, pp. 237–260, AGU, Washington D. C.

Strahler, A. (1964), Quantitative geomorphology of drainage basins and channel networks, in *Handbook of Applied Hydrology*, edited by V. Chow, pp. 439–476, McGraw-Hill, New York.

Tarboton, D. G. (1997), A new method for the determination of flow directions and contributing areas in grid digital elevation models, *Water Resour. Res.*, *33*(2), 309–319, doi:10.1029/96WR03137.

Tarboton, D. G., R. L. Bras, and I. Rodriguez-Iturbe (1992), A physical basis for drainage density, *Geomorphology*, *5*(1–2), 59–76, doi:10.1016/0169-555X(92)90058-V.

Tucker, G. E., and K. X. Whipple (2002), Topographic outcomes predicted by stream erosion models: Sensitivity analysis and intermodel comparison, *J. Geophys. Res.*, *107*(B9), 2179, doi:10.1029/2001JB000162.

Walcott, R. C., and M. Summerfield (2007), Scale dependence of hypsometric integrals: An analysis of southeast African basins, *Geomorphology*, *96*, 174–186.

Willgoose, G. (1994), A physical explanation for an observed area-slope-elevation relationship for catchments with declining relief, *Water Resour. Res.*, *30*(2), 151–159, doi:10.1029/93WR01810.

Willgoose, G., and G. Hancock (1998), Revisiting the hypsometric curve as an indicator of form and process in transport-limited catchment, *Earth Surf. Processes Landforms*, *23*(7), 611–623, doi:10.1002/(SICI)1096-9837(199807)23:7<611::AID-ESP872>3.0.CO;2-Y.

Willgoose, G., and H. Perera (2001), A simple model of saturation excess runoff generation based on geomorphology, steady state soil moisture, *Water Resour. Res.*, *37*(1), 147–155, doi:10.1029/2000WR900265.

Willgoose, G., R. L. Bras, and I. Rodriguez-Iturbe (1991), A physical explanation of an observed link area-slope relationship, *Water Resour. Res.*, *27*(7), 1697–1702, doi:10.1029/91WR00937.

Willgoose, G. R. (2001), Erosion processes, catchment elevations and landform evolution modelling, in *Gravel Bed Rivers V*, edited by M. P. Mosley, pp. 507–529, Hydrol. Soc., Wellington.

Wobus, C., K. Whipple, E. Kirby, N. Snyder, J. Johnson, K. Spyropolou, B. Crosby, and D. Sheehan (2006), Tectonics from topography: Procedures, promise and pitfalls, *Tectonics, Climate, and Landscape Evolution*, *Am. Penrose Spec. Pap.*, vol. 398, edited by S. D. Willett, N. Hovius, M. T. Brandon, and D. M. Fisher, pp. 55–74, Geol. Soc. of Am., Boulder, Colo.

S. Cohen and G. Willgoose, School of Engineering, University of Newcastle, Callaghan, NSW 2308, Australia. (g.willgoose@telluricresearch.com)

G. Hancock, School of Environmental and Life Sciences, University of Newcastle, Callaghan, NSW 2308, Australia.